Bibliographical reference

A Comparison of Frequency-Domain Microphone Array Methods for the Characterization of Rotating Broadband Noise Sources, Christof Ocker, Gert Herold, Florian Krömer, Wolfram Pannert, Ennes Sarradj and Stefan Becker, Acta Acustica **vol. 105** (Number 1), 2019, pp. 66-74

DOI

https://doi.org/10.3813/AAA.919288

Acta Acustica united with Acustica
Vol. 105 (2019) 66 – 74

DOI 10.3813/AAA.919288

A Comparison of Frequency-Domain Microphone Array Methods for the Characterization of Rotating Broadband Noise Sources

Christof Ocker[1)], Gert Herold[2)], Florian Krömer[3)], Wolfram Pannert[1)], Ennes Sarradj[2)], Stefan Becker[3)]

[1)] Aalen University, Beethovenstr. 1, 73430 Aalen, Germany. christof.ocker@hs-aalen.de

[2)] Technische Universität Berlin, Einsteinufer 25, 10587 Berlin, Germany

[3)] Friedrich-Alexander University Erlangen-Nürnberg, Cauerstr. 4, 91058 Erlangen, Germany

Summary

The localization and quantification of rotating sound sources is an important challenge in many fields of application. For the motion compensation of rotating sound sources, the two different frequency- domain microphone array methods 'virtual rotating array' and 'modal decomposition of the rotating sound field' are presented and compared to each other. At first, a simulated benchmark case with three discrete rotating broadband sound sources and a non-constant rotational speed is considered. The challenge is the reconstruction of the correct source positions and the source amplitudes. In a second case, a benchmark fan is analyzed to compare the source distribution and source amplitudes of the considered methods. Advantages, disadvantages and limits of the respective methods are shown.

PACS no. 43.60.Fg, 43.60.Jn

1. Introduction

The localization of rotating sound sources with a microphone array is a major task to reduce broadband axial fan noise. Depending on the adjusted operating point and considered frequency band, the sound sources are located at different parts of the fan blades [1, 2, 3, 4, 5]. Considerable effort has been put into compensating the relative motion of the sound sources to the microphone array and to understand the rotating sound source mechanism. The motion compensation thereby can be done in the time or the frequency domain. Sijtsma *et al.* [6] and Minck *et al.* [7] presented different methods in the time domain, taking into account the time delays and the Doppler effect due to the rotation. In their approach, the emitted signals from the moving sources are reconstructed by continuously moving the focus of the microphone array along the rotational motion of the fan. Other methods presented by Dougherty *et al.* [8], Herold and Sarradj [9], Lowis and Joseph [10] and Pannert and Maier [11] work in the frequency domain. For this, the pressure signals are Fourier transformed prior to the application of the beamforming algorithms. The motion compensation in the frequency domain can be done in different ways, e.g. by employing virtually rotating microphones or by a modal decomposition of the rotating sound field. The basic idea of the considered frequency-domain methods is the transformation of the recorded pressure signals into a rotating frame of reference and the correct calculation of the rotating sound field. To calculate the sound radiation of a rotating sound source, it should be kept in mind that in the rotating frame of reference, the medium between the microphone array and the sound sources is itself rotating. Ignoring the rotating medium will lead to inaccurate sound travel times between the assumed source positions and the microphones, as shown by Pannert and Maier [11].

For the considered methods, the microphones need to be arranged equidistantly on a ring, coaxial to the rotational axis of the sound sources. After the motion compensation, beamforming is used to localize the sound sources. High-resolution frequency-domain beamforming methods are based on the evaluation of the cross spectral matrix (CSM), which is approximated by averaging cross spectra of the time signals. Due to the averaging process, only stationary sources continuously emitting noise will remain dominant. By removing the main diagonal of the CSM, the influence of the uncorrelated background noise can be reduced [12]. Then, the CSM is multiplied with the steering vectors to shift the phase of the microphone signals according to the focus points.

The first method for motion compensation, that is used by Dougherty *et al.* [8], Herold *et al.* [9, 13], Zenger *et al.* [3, 14], and Krömer *et al.* [4, 5] defines a virtually rotating array. The pressure data at the virtual microphones are approximated through linear interpolation by the mea-

Received 2 May 2018,
accepted 1 November 2018.

sured signals according to the momentary angular position of the measured object. The cross spectra are calculated from the interpolated pressure signals and can be averaged with Welch's method. In contrast to this method, the method used by Lowis and Joseph [10], Pannert and Maier [11], and Ocker and Pannert [15], utilizes a modified free-space Green's function in the rotating frame of reference to describe the rotating sound field analytically. The modified Green's function is written as a summation of azimuthal modes, where each mode amplitude is a frequency-shifted counterpart of the expression for a stationary sound source. This frequency shift depends on the mode order and the rotational speed of the sound sources. In a second step, the pressure signals in the rotating frame of reference are calculated. Afterwards, the CSM in the rotating frame of reference is determined inversely from the calculated pressure signals in the rotating frame of reference. The averaging process of the reconstructed CSM is done in the frequency domain with Daniell's method [16].

The aim of this work is the comparison of the developed frequency-domain microphone array techniques for rotating broadband sound sources, particularly for the application on axial fans. Preliminary studies on this were done by Herold *et al.* [17] and Ocker *et al.* [18]. With these advanced techniques for the acoustic source characterization, optimization strategies can be developed to reduce the aeroacoustic sound emission. Usually, the sound source distribution on the rotating fan blades is not known. Therefore, the comparison of different sound source localization methods for rotating applications helps to produce reliable results for the sound source distribution and the source amplitudes.

The paper is organized as follows. The theory section features a summary of the methods of motion compensation including the calculation of the CSM and the Clean-SC deconvolution method. In the setup section, a description of the two considered benchmark cases is given. Then, the obtained results for the different methods of motion compensation are compared to each other and discussed. The conclusions are drawn in the last section.

2. Theory

The data processing for the localization of rotating sound sources with a microphone array follows the descriptions by Herold and Sarradj [9] for the virtual rotating array method, Pannert and Maier [11] for the modal decomposition method, Ocker and Pannert [16] for the calculation of the CSM with Welch's and Daniell's method, and Sijtsma [12] for the Clean-SC deconvolution method.

For the localization of rotating sound sources with a microphone array, two major tasks have to be fulfilled:

- calculation of the CSM in the rotating frame of reference from the pressure signals at the microphones in the rotating frame of reference and
- consideration of the rotating medium between the microphone array and the sound sources in the rotating frame of reference.

The Clean-SC deconvolution method is exactly the same as for stationary sound sources. For the motion compensation of rotating sound sources, the microphones need to be arranged equidistantly on a circular array, which is aligned coaxial to the axis of rotation. The methods can be extended for the use of several rings of microphones [5].

2.1. Virtual rotating array

Using the virtual rotating array method (VRA), the measured time data from the stationary system are transformed into a rotating frame of reference that rotates synchronously with the sound sources. Dougherty *et al.* [8] recommended the number of virtually rotating microphones L_{virt} to match the number of physical microphones L approximately to avoid an unrealistic high angular resolution. The virtual microphone coordinates no longer correspond to the coordinates of the physical microphones. To compensate a potentially varying rotational speed, the source position is tracked revolution by revolution and recorded synchronously to the microphone data. The pressure signals at the virtual microphone positions are then calculated by linear interpolation from the measured sound pressures. After the interpolation, the time data are transformed into the frequency domain using Welch's method [19]. Therefore, the time signal for each virtual microphone is divided into overlapping time blocks, onto which a fast Fourier transformation (FFT) is applied. The CSM $\mathbb{C}$ is the result of the cross correlated pressure signals $\boldsymbol{P}_{\mathrm{virt}}$ of all possible pairs of virtual microphones,

$$\mathbb{C} = \overline{\boldsymbol{P}_{\mathrm{virt}} \boldsymbol{P}_{\mathrm{virt}}^{H}}, \tag{1}$$

where the superscript H indicates the Hermitian transpose.

For the compensation of the rotating medium in the rotating frame of reference, the travel distances for the calculation of the steering vectors are corrected. For the correction, the effective travel distance/travel time of each microphone-focus point combination is adapted, taking into account that the virtual microphones and the focus points are rotating, but the medium – at a first approximation – is not. The effective sound travel distance as required for the steering vector calculation is obtained by rotating the microphone positions such that after a time δt, the distance from a focus point to a new microphone position, rotated by the increment

$$\delta\varphi = \Omega \delta t, \tag{2}$$

with Ω being the average rotational frequency, corresponds to the travel distance of the sound wave [5]. This effective distance is then used for the steering vector calculation.

2.2. Modal decomposition

As an alternative to the VRA, the modal decomposition method (MD) can be used. For this method, the first step

is to transform the pressure signals at the stationary microphones from the time domain into the frequency domain via an FFT. The sound field of a rotating point source in the rotating frame of reference is then defined as

$$\boldsymbol{P}_\Omega = \mathbb{G}_\Omega \boldsymbol{Q}. \tag{3}$$

$\boldsymbol{P}_\Omega$ is a complex vector with the frequency-domain pressure signals in the rotating frame of reference. The dimension of this vector is the number of microphones. $\boldsymbol{Q}$ is a vector with the real part of the unknown sound pressures. Since the positions of the sound sources are not known, a focus plane is defined parallel to the microphone array plane. The focus plane is discretized with an equally-spaced Cartesian grid. For each grid point the sound pressure is calculated. Therefore, the dimension of $\boldsymbol{Q}$ is the number of grid points. $\mathbb{G}_\Omega$ is a complex matrix with the modal decomposed Green's function, which describes the sound radiation of a rotating sound source in the rotating frame of reference. The dimension of the matrix is the number of microphones by the number of grid points on the focus plane.

To compensate the source motion, it is necessary to shift the coefficients of the azimuthal modes $\boldsymbol{P}_m$ of the pressure signals according to

$$\boldsymbol{P}_\Omega(r_l, \varphi_l, \Theta_l, \omega) = \sum_{m=-\frac{L}{2}}^{+\frac{L}{2}} \boldsymbol{P}_m(r_l, \Theta_l, \omega_0 + m\Omega)\, \mathrm{e}^{\mathrm{i}m\varphi_l}, \tag{4}$$

where m is the mode order, Ω the rotational frequency, ω_0 is the angular frequency of the sound source pulsation and r_l, φ_l and Θ_l are the radial distance, the azimuthal angle and the polar angle of the l-th microphone in the rotating frame of reference respectively. The number of microphones of the array limits the resolution of the propagating azimuthal modes m. According to Poletti [20], the negative limit of azimuthal modes to be considered can be approximated as

$$m^- = \frac{-k_0 r_s}{1 + k_R r_s} \tag{5}$$

and the positive limit as

$$m^+ = \frac{k_0 r_s}{1 - k_R r_s}. \tag{6}$$

Here, r_s is the maximum sound source radius, $k_0 = \omega_0/c$ the wave number of the emitted frequency of the sound source and $k_\mathrm{R} = \Omega/c$ the wave number due to the rotation. For the definition of the number of microphones to be used for actual measurements, the number of propagating azimuthal modes has to be resolved. The number of propagating azimuthal modes can be determined by Equation (5) and Equation (6). Positive azimuthal modes correspond to co-rotating modes and negative azimuthal modes to counter-rotating modes. Objects with non-constant rotational speed can be investigated by analyzing short time sequences and averaging over these sequences.

After the motion compensation, the CSM can be calculated from the pressure signals in the rotating frame of reference $\boldsymbol{P}_\Omega$. The CSM is calculated similar to Equation (1) as

$$\mathbb{C} = \overline{\boldsymbol{P}_\Omega \boldsymbol{P}_\Omega^H}. \tag{7}$$

In contrast to the virtual rotating array method, averaging the CSM with Welch's method is not practicable, because a high-resolution spectrum is needed to determine the correct frequency $\omega_0 + m\Omega$ in Equation (4). Hence the CSM is calculated in the frequency domain with Daniell's method [21]. In contrast to Welch's method, the time signal is not divided into smaller time blocks with Daniell's method. The FFT is applied on the complete time signal for the calculation of a high-resolution spectrum. In a second step, a spectral window is used to sum up the energy of the high-resolution spectrum around the analyzed frequency components. In contrast to tonal sound sources, the energy of the frequency components for broadband sound sources have to be summed up and not averaged. A comparison of the calculation of the CSM with Welch's and Daniell's method is shown by Ocker and Pannert [16].

To compensate the rotating medium in the rotating frame of reference, the modal decomposed Green's function is used. The modal decomposed Green's function in the rotating frame of reference in spherical coordinates is defined as

$$\begin{aligned}\mathbb{G}_\Omega(r_l, \varphi_l, \Theta_l, r_s, \varphi_s, \Theta_s, \omega) = \\ \mathrm{i}\sum_{n=0}^{+\infty}\sum_{m=-n}^{n} k_m \mathrm{e}^{\mathrm{i}m(\varphi_{l0}-\varphi_{s0})} j_n(|k_m| r_<) \\ \cdot\, h_n^{(\delta_m)}(|k_m| r_>) Y_n^m(\Theta_l, \varphi_l) Y_n^m(\Theta_s, \varphi_s)^*,\end{aligned} \tag{8}$$

where $k_m = (\omega_0 + m\Omega)/c$ is the wave number of the acoustic mode m accounting for the frequency shift due to the source rotation Ω. r_s, φ_s and Θ_s are the time-independent source position coordinates evaluated in the rotating frame of reference. $j_n(\cdot)$ is the first kind of the n-th spherical Bessel function, $h_n^{(\delta_m)}(\cdot)$ is the spherical Hankel function of the order n and the kind δ_m is defined as

$$\delta_m = \begin{cases} 2 & \text{for} \quad k_m \geq 0 \\ 1 & \text{for} \quad k_m < 0 \end{cases}. \tag{9}$$

$r_<$ is the smaller radius of r_l and r_s, and $r_>$ is the larger one [22]. $Y_n^m(\cdot)$ are the normalized spherical harmonics

$$Y_n^m(\theta, \varphi) = \sqrt{\frac{(2n+1)}{4\pi}\frac{(n-|m|)!}{(n+|m|)!}} P_n^{|m|}(\cos\theta) \mathrm{e}^{\mathrm{i}m\varphi}. \tag{10}$$

$P_n^{|m|}$ is the associated Legendre function of the first kind of degree n and order m and the superscript * denotes the complex conjugation.

The modified Green's function compensates the rotating medium in the rotating frame of reference and serves as transfer function used in the steering vector calculation.

Due to the complexity of the necessary calculations, it can be expected that the MD method is computationally more costly than the VRA method. However, a direct comparison of calculation times was not done in this study.

2.3. Beamforming and Deconvolution

After the CSM is obtained, beamforming algorithms and the Clean-SC deconvolution method can be applied. Most commonly, the amplitude of the considered focus point B_s is calculated in the frequency domain by the delay-and-sum beamformer as

$$B_s = \boldsymbol{h}_s^H \mathbb{C} \boldsymbol{h}_s, \tag{11}$$

where h_s is the steering vector for a specific focus point s. Sarradj [23] showed that known steering vector formulations always make a small error in the calculation of either the source positions or pressure amplitudes. The steering vector formulation in this paper is normalized to the pressure amplitude, which corresponds to formulation III in the work of Sarradj [23]. Based on the delay-and-sum beamformer output B_s, the Clean-SC deconvolution method searches for the highest peak and transfers it into an empty (clean) map. In a second step, all coherent portions to the highest peak are identified and subtracted from the original (dirty) map. The highest peaks from the dirty map are identified iteratively and copied to the clean map until no more significant sources are found or a maximum number of iterations is reached [12].

3. Setup and results

For the comparison of different data processing approaches (VRA and MD) for localizing rotating sound sources with a microphone array, two benchmark cases are investigated. First, the simulated benchmark case by Herold [24] is considered. Three point sources with different source levels are rotating clockwise with the same, but temporally slightly varying rotational speed and emit uncorrelated white noise. The challenge is to determine the correct position and the sound pressure level of each of the three sources at the trigger instant [17]. To focus the sound sources correctly, the non- constant rotational speed has to be considered. In the second benchmark case by Zenger *et al.* [25], a generic fan with unskewed fan blades is investigated. Here, the pressure signals from the axial fan N1UG are measured with a microphone array for a specific operating point [3]. The challenge is to localize the unknown source distribution and to determine the sound pressure level at the fan blades for different frequency bands. The two benchmarks are very similar to each other concerning the microphone array configuration and the measurement distance from the sound sources to the microphone array. Both benchmarks are freely available. The data sets have been created to enable comparisons between different microphone array analysis methods or implementations.

3.1. Three rotating sound sources

The time data are generated at 64 microphone positions. The microphones are equidistantly distributed on a ring with a diameter of 1 m, which is placed axisymmetric to the axis of rotation of the sound sources. The sampling frequency is $f_{\text{sample}} = 48\,\text{kHz}$, the evaluation time

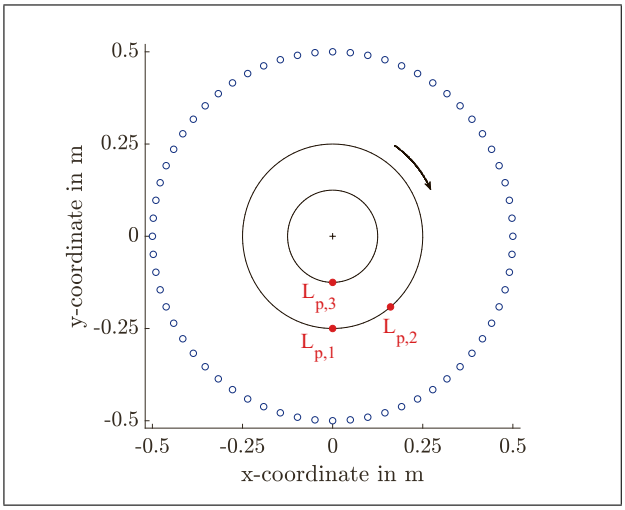

Figure 1. (Colour online) Positions of the three sources at a trigger instant (red markers) and positions of the 64 microphones (blue markers).

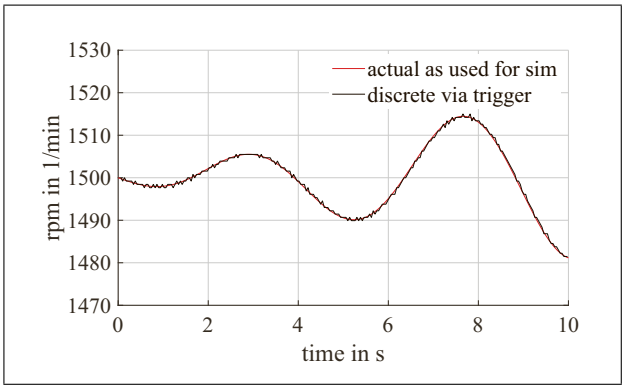

Figure 2. Non-constant rotational rate.

$t_{\text{eval}} = 10\,\text{s}$ and the distance from the sources to the microphone array $z = 0.5\,\text{m}$. The rotation is tracked by a one-trigger-per-revolution signal. Figure 1 shows the positions of the sources (red markers) at the trigger instant and the microphone array (blue markers). The source levels are $L_{p,1} = L_{p,2} + 3\,\text{dB} = L_{p,3} + 6\,\text{dB}$.

Figure 2 shows the non-constant rotational rate as a function of the evaluation time.

The focus plane is discretized with an equally-spaced Cartesian grid consisting of 61 × 61 points with 0.01 m spacing. The resulting total area of the focus plane is 0.6 m × 0.6 m. The analysis is performed with the Clean-SC deconvolution method with a loop gain of 0.9. While the calculations of the CSM and steering vectors differ depending on the method, the Clean-SC implementation used in each case is identical. This has been done by exporting the CSM and the corresponding steering vectors of each motion compensation method and calculating the beamforming source map with the same Clean-SC implementation.

The sound maps are evaluated for the third octave band having a center frequency $f_c = 2500\,\text{Hz}$ and plotted with a dynamic range of 20 dB. Assuming an averaged constant rotational rate of $n = 1500\,\text{rpm}$ over the entire evaluation

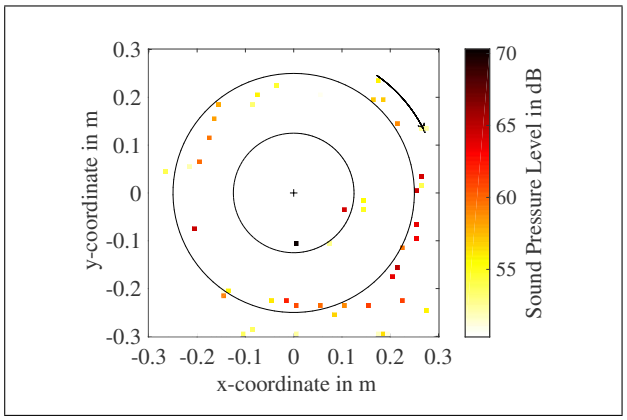

Figure 3. Smeared sound source distribution assuming a constant rotational rate for the third octave band having a center frequency $f_c = 2500$ Hz.

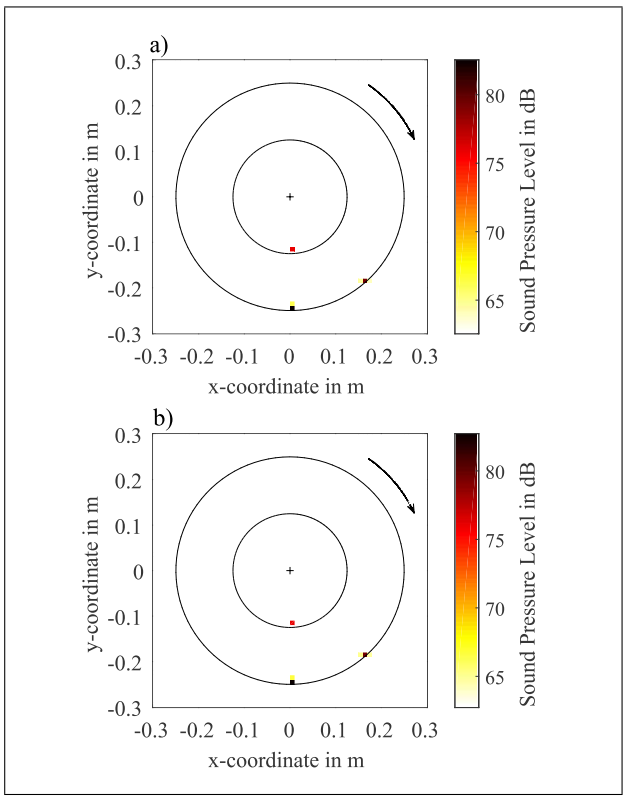

Figure 4. Correct focused sound sources with a) the VRA and b) the MD for the third octave band having a center frequency $f_c = 2500$ Hz.

time leads to a smeared beamforming source map: The number of sound sources, the positions and sound pressure levels cannot be determined, as is shown in Figure 3.

For correctly-focused sound sources, the varying rotational speed has to be taken into account. To produce the beamforming map in Figure 4a, the VRA is used for motion compensation and Welch's method for calculating the CSM. The beamforming map in Figure 4b is generated with the MD for motion compensation and Daniell's method for calculating the CSM.

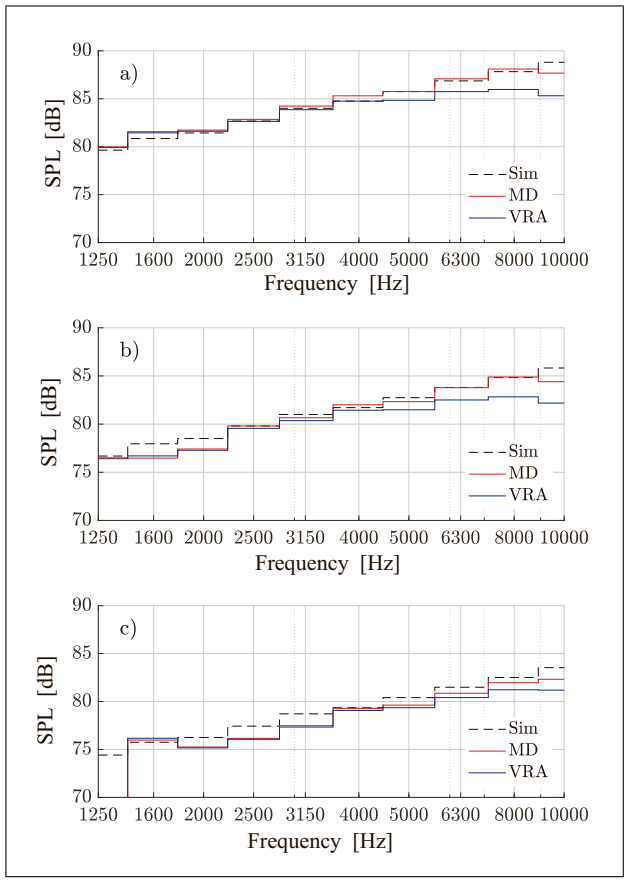

Figure 5. Integrated spectra for the three rotating sources calculated with VRA (blue) and MD (red): a) Source $L_{p,1}$, b) Source $L_{p,2}$, c) Source $L_{p,3}$.

For this benchmark case, the results look very similar, with a maximum deviation of < 1 dB between the reconstructed amplitudes, although the method of motion compensation and averaging the CSM are different. The two considered methods VRA and MD yield comparable results in terms of localization of the rotating sound sources and calculation of the sound pressure levels.

For a quantitative analysis of the source reconstruction performance of the methods, source spectra are calculated by integrating sound maps over the focus points contained in a circular area around each of the three sources. The diameter of these integration areas is 0.05 m. Figures 5a-c show the integrated spectra for the individual sources. The dashed black line is the correct spectral distribution, as used for generating the microphone signals.

The sound pressure levels of all three sound sources are reconstructed well in the frequency range between 1250 Hz and 5000 Hz. Below 1250 Hz the resolution of stationary and rotating sound sources is limited. Following the work of Dougherty *et al.* [26] the minimum resolvable distance of two point sources of equal strength can be determined by the Sparrow limit,

$$r_{\text{min,Clean-SC}} = 0.96 \cdot 0.47 \cdot \frac{\lambda}{\sin(\Theta)}, \qquad (12)$$

where λ is the wave length and Θ is the half-angle under which the array aperture is seen from a focus point.

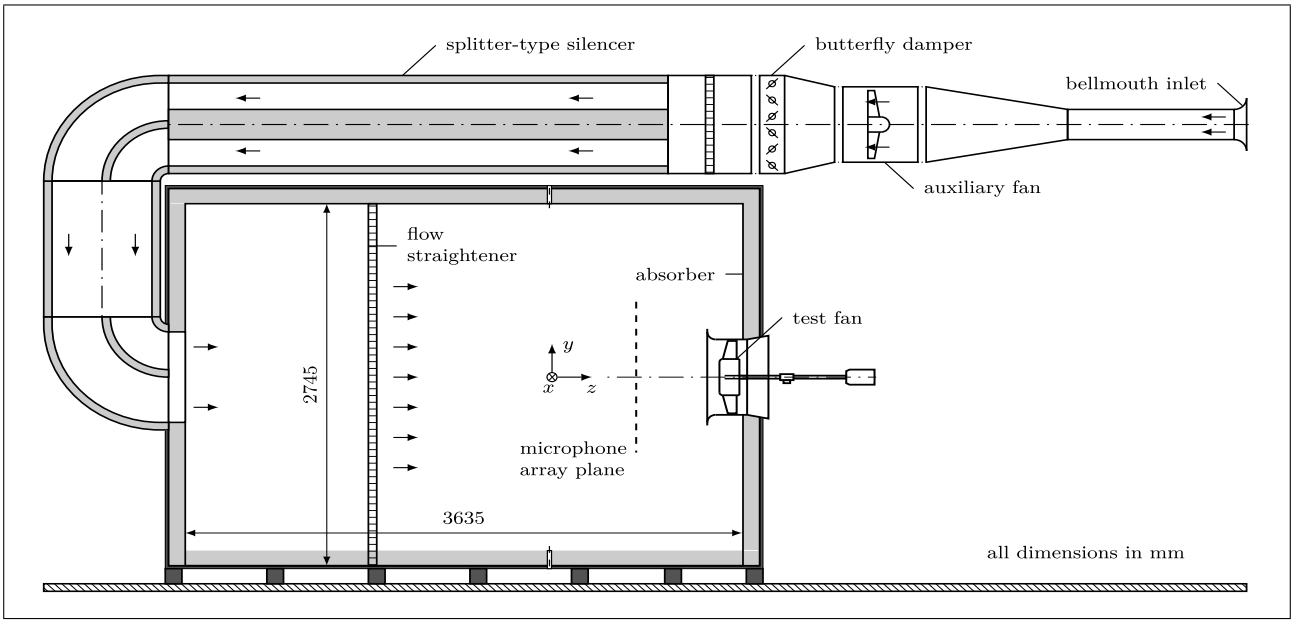

Figure 6. Standardized inlet test chamber based on ISO 5801.

While the calculated levels may deviate slightly from the theoretic levels, both methods yield almost the same values. At 1250 Hz, Clean-SC fails to detect the weakest source for both methods. At frequencies between 6300 Hz and 10000 Hz, the sound pressure levels calculated with the MD method are closer to the expected levels than those calculated with the VRA method, which underestimates the level more and more significantly with higher frequencies. The apparent better performance of MD may be explained by this method using the signals of all microphones to approximate a signal at any of the positions in the rotating frame, while VRA calculates these signals exclusively from linear interpolation between adjacent microphones. At 10000 Hz, both methods underestimate the sound pressure levels of the three sound sources. The necessary number of microphones depends on the frequency band of interest. As shown in earlier studies [17, 18], the use of too few microphones leads to different errors depending on the method. With the VRA method, energy leaks into focus points neighboring the actual source position. As the number of microphones directly limits the number of resolvable modes, with MD, energy from higher modes leaks into used modes, which leads to method-characteristic artifacts. Thus, while MD appears to be more robust dealing with higher frequencies than VRA, to correctly reconstruct the sources at 10000 Hz, the number of microphones would have to be increased for both methods.

3.2. Low-pressure axial fan N1UG

The benchmark is performed on a generic fan with unskewed fan blades. The experimental setup of the benchmark as well as the aerodynamic performance of the fan, fluid mechanical quantities from laser Doppler anemometer (LDA) measurements, wall pressure fluctuations in the gap region and sound characteristics are described in detail by Zenger et al. [25, 27]. The unskewed test fan is mounted in a short duct and integrated into a standardized anechoic inlet test chamber based on ISO 5801 [28], as shown in Figure 6. A detailed description of the test fan and the measurement setup is provided in [5].

Table I. Fan design parameters.

Parameter	Value
Rotor diameter D	495 mm
Hub diameter D_{hub}	248 mm
Tip gap s_{tip}	2.5
Number of blades z	9
Rotational rate n	24.8 Hz
Flow rate coefficient ϕ	0.18
Total-to-static pressure coefficient ψ_{ts}	0.18

The fan design parameters are listed in Table I.

The flow rate coefficient ϕ and the total-to-static pressure coefficient ψ_{ts} are defined as

$$\phi = \frac{4\dot{V}}{\pi^2 D^3 n} \tag{13}$$

and

$$\psi_{ts} = \frac{2\Delta p_{ts}}{\rho(\pi D n)^2}, \tag{14}$$

where $\dot{V}$ is the volume flow rate, D the fan diameter, n the rotational speed in clockwise direction as seen in Figure 7, Δp_{ts} the total-to-static pressure difference and ρ the air density.

To determine the angular position of the fan, an optical fork sensor (one 3 V pulse per revolution) is used. The measurement is carried out with 64 microphones arranged

Figure 7. Generic test fan (rotational direction: clockwise) and microphone array.

on a ring-shaped array that is mounted axisymmetric to the rotation axis of the fan. Figure 7 shows the arrangement of the microphones of the type 40PH-Sx (G.R.A.S. Sound and Vibration A/S) on a ring with a diameter of $D_{array} = 1$ m. The distance from the microphone array to the fan is 0.49 m.

The sampling frequency of the measured pressure signals is $f_{sample} = 48$ kHz, recorded with a PXIe-1075 front end with PXIe-4496 data acquisition modules (National Instruments Corporation). The evaluation time is $t_{eval} = 20$ s, which corresponds to 500 fan revolutions. Similar to the evaluations for the previous benchmark problem, the focus plane is discretized with an equally-spaced Cartesian grid consisting of 61 × 61 points with 0.01 m spacing. The total area of the focus plane is 0.6 m × 0.6 m. The analysis is performed with the Clean-SC deconvolution method with a loop gain of 0.9. For the sound maps, a dynamic range of 20 dB is used. The beamforming map evaluated with the VRA is shown in Figure 8a and the beamforming map evaluated with the MD is shown in Figure 8b for the third octave band having a center frequency $f_c = 2500$ Hz.

In this frequency band, the main sound sources are located in the tip region near the leading edge. This is reasonable, as the circumferential velocity increases from hub to tip, which leads to a stronger interaction mechanism of the fan blade leading edges with the inflow [4, 29, 30]. Even though there were no obstructions upstream of the fan, sound sources are anticipated in the leading edge region as the inflow generally holds a certain degree of turbulence intensity, even under free inflow conditions. Furthermore, the tip leakage flow leads to an unsteady flow field in the tip region, in particular for unskewed fans, with greatly increased turbulence intensity levels [5, 31, 32].

In Figure 9 the same evaluation is presented for the third octave band having a center frequency $f_c = 5000$ Hz.

The sound sources are distributed from the fan blade leading to the fan blade trailing edge. The high-frequency sound radiation of low-pressure axial fans is usually dom-

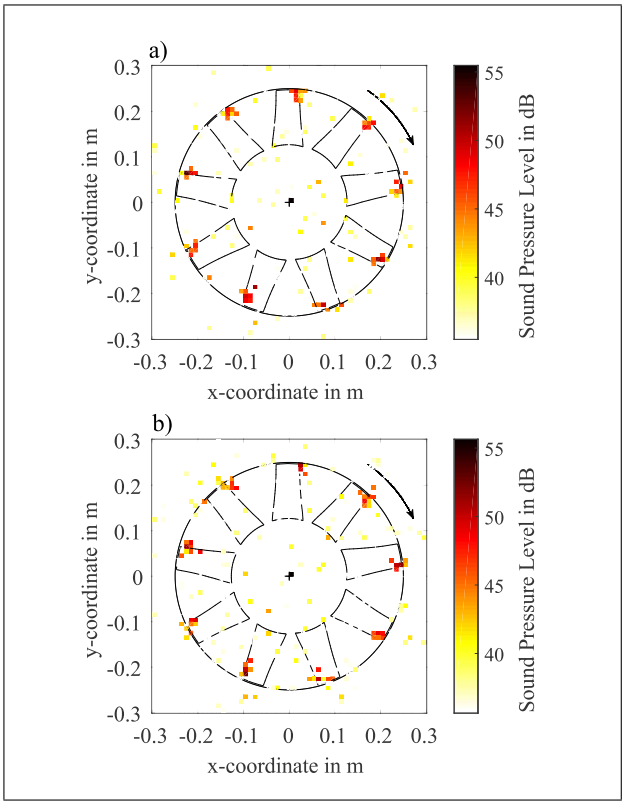

Figure 8. Beamforming sound maps of the fan N1UG evaluated with a) the VRA and b) the MD for the third octave band having a center frequency $f_c = 2500$ Hz.

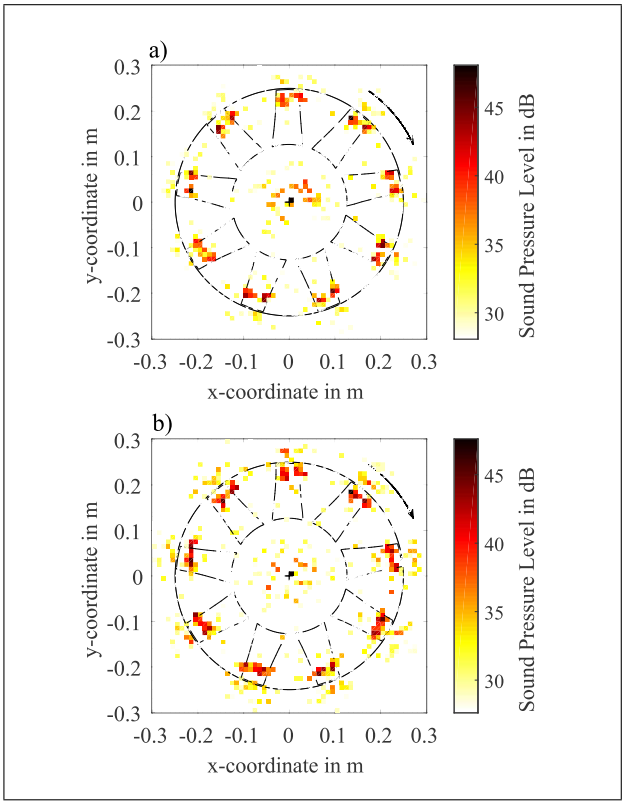

Figure 9. Beamforming sound maps of the fan N1UG evaluated with a) the VRA and b) the MD for the third octave band having a center frequency $f_c = 5000$ Hz.

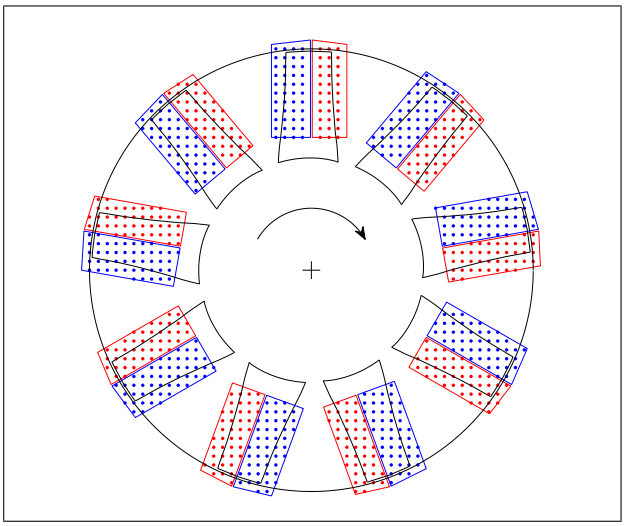

Figure 10. (Colour online) Leading edge subregions (red) and trailing edge subregions (blue) for the integrated spectra.

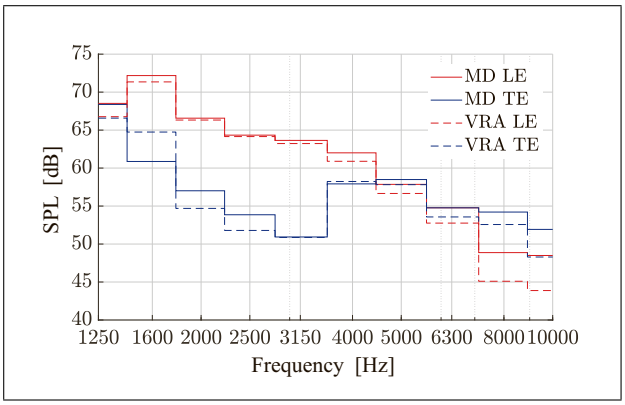

Figure 11. (Colour online) Leading edge subregions (LE, red) and trailing edge subregions (TE, blue) spectra as calculated with VRA (dashed lines) and MD (solid lines).

inated by trailing edge noise [33, 34]. Accordingly, it can be seen that the sound sources shift partly to the fan blade trailing edge regions. The sound sources in the leading edge regions are an indicator for a highly unsteady flow field in the tip region, as mentioned before. It can be recognized that both motion compensation methods – VRA and MD – are capable of distinguishing between the different sound sources, even though the chord length is only $l_c \approx 70\,\text{mm}$ at the fan blade tip.

In a second step, the fan blades are separated into two integration regions, such that the sound pressure levels are integrated over the leading edge subregions and the trailing edge subregions for both methods. The subregions for the leading edge (red) and for the trailing edge (blue) are shown in Figure 10.

In Figure 11, the integrated spectra are shown for the VRA and the MD motion compensation methods. The spectral characteristics of the individual subregions of the same respective type – leading or trailing edges – are quite similar [3, 13]. For this reason and for clarity, the displayed leading and trailing edge spectra are calculated by summing the sound pressure levels in the corresponding subregions of all blades.

Both methods yield spectral curves with similar general characteristics. Below 1250 Hz, the beamforming sound maps do not yield reliable results for the sound source distribution due to the array aperture. In this case the Sparrow limit calculates to approximately 0.2 m for 1000 Hz, which exceeds even the distances of the blade tips [3]. In the frequency range between 1250 Hz and 4000 Hz, the dominant sound sources are located in the area of the leading edges. Above 4000 Hz, the dominating sound sources move towards the trailing edges. Similar trends have been observed in previous studies [3, 5].

In the frequency range between 1250 Hz and 4000 Hz the sound pressure levels at the leading edge subregions are similar for VRA and MD. For the trailing edge subregions, the integrated sound pressure levels differ considerably depending on the method: At 1600 Hz, the level calculated using VRA is 4 dB above the MD level, while at 2000 Hz and 2500 Hz, MD calculates trailing edge noise levels to be 2 dB above the VRA level. Whether these differences stem from the different calculation methods of the CSM (VRA–Welch / MD–Daniell) or the general properties of the methods is unclear at this point and should be subject of further investigations. Above 4000 Hz, MD calculates slightly higher sound pressure levels for the leading and trailing edge subregions than VRA. As a similar phenomenon could be observed with simulated data (see section 3.1), this effect can be assumed to be due to the interpolation error made by the VRA method. As can be seen in the sound maps, the source distributions for both methods show comparable results in terms of the localization of the sound sources at different frequency bands. In general, both motion compensation methods are capable of resolving rotating broadband sound sources in a real application case.

4. Conclusion

The virtual rotating array method and the modal decomposition method, which aim to compensate the rotational movement of rotating sound sources, are presented and compared to each other. Two benchmark cases are considered for the assessment of rotating sound sources. At first, a simulated case with discrete rotating broadband sound sources with a non- constant rotational speed is analyzed. Secondly, an application with an unskewed low-pressure axial fan and distributed sound sources is considered. Integrated spectra are calculated for a quantitative analysis of the source reconstruction performance of the methods. Both methods correctly identify the positions and the sound pressure levels of the simulated benchmark with three rotating sound sources at various frequency bands. In the experimental benchmark case, both methods yield consistent results for the unknown sound source distribution on the axial fan. A trend is identified in both benchmark cases, that for frequencies above 4000 Hz, MD calculates higher sound pressure levels in all third octave

bands than VRA for the dominating and less significant sound sources. For both methods the evaluable upper frequency depends on the number of microphones used. For the MD method, this limit appears to be about two one-third octave bands above that of the VRA method. Below 4000 Hz, comparable results could be obtained for simulated and measured sound sources. This investigation shows that both frequency-domain microphone array methods are well suited for characterizing rotating broadband sound sources.

References

[1] S. Wright: The acoustic spectrum of axial flow machines. Journal of Sound and Vibration **45** (1976) 165–223.

[2] T. Carolus: Ventilatoren. Vieweg+Teubner Verlag, 2013.

[3] F. Zenger, G. Herold, S. Becker, E. Sarradj: Sound source localization on an axial fan at different operating points. Experiments in Fluids **57** (2016).

[4] F. Krömer, J. Müller, S. Becker: Investigation of aeroacoustic properties of low-pressure axial fans with different blade stacking. AIAA Journal **56** (2018) 1507–1518.

[5] F. Krömer: Sound emission of low-pressure axial fans under distorted inflow conditions. FAU University Press, 2018.

[6] P. Sijtsma, S. Oerlemans, H. Holthusen: Location of rotating sources by phased array measurements. 7th AIAA/CEAS Aeroacoustics Conference and Exhibit, 2001, American Institute of Aeronautics and Astronautics.

[7] O. Minck, N. Binder, O. Cherrier, L. Lamotte, V. Pommier-Budinger: Fan noise analysis using a microphone array. Fan 2012 - International Conference on Fan Noise, Technology, and Numerical Methods, Senlis, FR, 2012, pp. 1–9.

[8] R. Dougherty, B. Walker, D. Sutliff: Locating and quantifying broadband fan sources using in-duct microphones. 16th AIAA/CEAS Aeroacoustics Conference, 2010, American Institute of Aeronautics and Astronautics.

[9] G. Herold, E. Sarradj: Microphone array method for the characterization of rotating sound sources in axial fans. Noise Control Engineering Journal **63** (2015) 546–551.

[10] C. Lowis, P. Joseph: Determining the strength of rotating broadband sources in ducts by inverse methods. Journal of Sound and Vibration **295** (2006) 614–632.

[11] W. Pannert, C. Maier: Rotating beamforming – motion-compensation in the frequency domain and application of high-resolution beamforming algorithms. Journal of Sound and Vibration **333** (2014) 1899–1912.

[12] P. Sijtsma: Clean based on spatial source coherence. International Journal of Aeroacoustics **6** (2007) 357–374.

[13] G. Herold, F. Zenger, E. Sarradj: Influence of blade skew on axial fan component noise. International Journal of Aeroacoustics **16** (2017) 418–430.

[14] F. Zenger, G. Herold, S. Becker: Acoustic characterization of forward- and backward-skewed axial fans under increased inflow turbulence. AIAA Journal **55** (2017) 1241–1250.

[15] C. Ocker, W. Pannert: Imaging of broadband noise from rotating sources in uniform axial flow. AIAA Journal **55** (2017) 1185–1193.

[16] C. Ocker, W. Pannert: Calculation of the cross spectral matrix with daniell's method and application to acoustical beamforming. Applied Acoustics **120** (2017) 59–69.

[17] G. Herold, C. Ocker, E. Sarradj, W. Pannert: A comparison of microphone array methods for the characterization of rotating sound sources. BeBeC-2018-D22, 7th Berlin Beamforming Conference, 2018.

[18] C. Ocker, G. Herold, F. Krömer, W. Pannert, E. Sarradj, S. Becker: Comparison of microphone array methods for the characterization of rotating broadband noise sources. FAN2018, 2018.

[19] P. Welch: The use of fast fourier transform for the estimation of power spectra: A method based on time averaging over short, modified periodograms. IEEE Transactions on Audio and Electroacoustics **15** (1967) 70–73.

[20] M. A. Poletti: Series expansions of rotating two and three dimensional sound fields. The Journal of the Acoustical Society of America **128** (2010) 3363–3374.

[21] P. J. Daniell: Discussion on "symposium on autocorrelation in time series". Journal of the Royal Statistical Society **Supplement** (1946) 88–90.

[22] M. A. Poletti, P. D. Teal: Comparison of methods for calculating the sound field due to a rotating monopole. The Journal of the Acoustical Society of America **129** (2011) 3513–3520.

[23] E. Sarradj: Three-dimensional acoustic source mapping with different beamforming steering vector formulations. Advances in Acoustics and Vibration **2012** (2012) 1–12.

[24] G. Herold: b11 - rotating point sources. 2017. https://www.b-tu.de/fg-akustik/lehre/aktuelles/arraybenchmark.

[25] F. Zenger, C. Junger, M. Kaltenbacher, S. Becker: A benchmark case for aerodynamics and aeroacoustics of a low pressure axial fan. SAE Technical Paper Series, 2016, SAE International.

[26] R. P. Dougherty, R. C. Ramachandran, G. Raman: Deconvolution of sources in aeroacoustic images from phased microphone arrays using linear programming. International Journal of Aeroacoustics **12** (2013) 699–717.

[27] European Acoustic Association: Benchmark cases for computational acoustics. 2018. https://eaa-bench.mec.tuwien.ac.at/benchmarks/acoustics_involving_heterogeneous_and_moving_fluids/axial_fan/.

[28] International Organization for Standardization: ISO 5801: 2007 Industrial fans - performance testing using standardized airways. 2007.

[29] F. Agboola, T. Wright: The effects of axial fan noise control by blade sweep on the radial component of velocity. 5th AIAA/CEAS Aeroacoustics Conference and Exhibit, 1999, American Institute of Aeronautics and Astronautics.

[30] T. Fukano, C.-M. Jang: Tip clearance noise of axial flow fans operating at design and off-design condition. Journal of Sound and Vibration **275** (2004) 1027–1050.

[31] T. Zhu, D. Lallier-Daniels, M. Sanjosé, S. Moreau, T. Carolus: Rotating coherent flow structures as a source for narrowband tip clearance noise from axial fans. Journal of Sound and Vibration **417** (2018) 198–215.

[32] S. Moreau, M. Sanjose: Sub-harmonic broadband humps and tip noise in low-speed ring fans. The Journal of the Acoustical Society of America **139** (2016) 118–127.

[33] W. K. Blake: Mechanics of flow-induced sound and vibration: Complex flow-structure interactions. Vol. 2, Chapter 11-12. Academic Press, New York, 1986.

[34] S. Wagner, R. Bareiß, G. Guidati: Wind turbine noise. Springer Berlin Heidelberg, 1996.